PCCP
Physical Chemistry Chemical Physics

Accepted Manuscript

This article can be cited before page numbers have been issued, to do this please use: M. Monwar, P. Mondol, C. Barile, T. Jalil, R. Tung, D. Hanigan, M. Shamim Al Mamun and M. R. Khan, *Phys. Chem. Chem. Phys.*, 2026, DOI: 10.1039/D5CP00185D.

View Article Online
DOI: 10.1039/D5CP00185D

ARTICLE

Investigating Physico-chemo-mechanical Changes of Eutectic Gallium Indium (eGaIn) Thin Films Induced by Fluorinated Aqueous Droplets

Received 00th January 20xx,
Accepted 00th January 20xx

DOI: 10.1039/x0xx00000x

Momena Monwar,[a] Profulla Mondal,[b] Christopher J. Barile,[b] Md Tasmirul Jalil,[c] Ryan C Tung,[c] David Hanigan,[d] Muhammad Shamim Al Mamun,[a] and M. Rashed Khan*[,a]

Herein, we demonstrate how the chemical sensitivity and mechanical stability of 2D thin films of eutectic gallium indium (eGaIn) can be leveraged to sense the presence of dilute amounts of fluorinated compounds (e.g., per- and polyfluorinated alkyl substances or PFAS). The method utilizes the interfacial interactions between 2D thin films of eGaIn and PFAS microdroplets, which induce thin film delaminations due to the perturbations in the Ga-to-O ratio at the interface. We tested three fluorinated samples – 200 ppm perfluorooctanoic acid (PFOA), 0.014 ppb PFAS, and 0.001 ppb PFAS to investigate the delamination, which exhibits sensitivities to concentrations. We leveraged energy-dispersive X-ray spectroscopy (EDS) and Raman spectroscopy to quantify and probe the shift in elemental distributions and surface dynamics of the eGaIn films. The observed delamination phenomena and the spectroscopic analyses suggest that our method provides a rapid *in situ* PFAS analysis tool related to total organic fluorine detection, complementing the existing technologies. Such a simplistic tool offers a fast approach to developing low-cost, field-deployable chemical sensors for total organofluorine detection.

Introduction

This article aims to demonstrate a proof-of-principle method to detect the presence of dilute fluorinated compounds, leveraging the mechanical stability and chemical sensitivity of a 2D thin film of eutectic gallium indium (eGaIn[1,2]), an alloy of gallium-based liquid metals (LM[3]). LM alloys of gallium (Ga) have garnered interest among the scientific community due to their low melting points, high conductivity, low fluidity, and, most importantly, their stable surface oxide layer, which readily forms in native air.[3] The surface of LM alloys is readily oxidized in air, producing a ~3 nm gallium oxide (Ga_2O_3), which is amphoteric and passivating.[4–6] This Ga_2O_3 layer gives the bulk metal mechanical stability to produce 3D microsystems and 2D thin films. [7–9] Numerous studies have reported methods to etch and deposit [10–12] the surface oxide and control the shape of the bulk metal to demonstrate shape-reconfigurable systems.[6,13,14] However, studies on harnessing the chemical sensitivity and mechanical stability of a 2D thin film as a probe to analyze aqueous droplets have remained untapped. Herein, we report the feasibility of 2D thin films of eGaIn for interface-enhanced studies of microdroplets of fluorinated substances.

The presence of per- and polyfluoroalkyl substances (PFAS) in water has new regulatory limits set by the Environmental Protection Agency (EPA) to ensure water quality, environmental health, safe industrial processes, and human well-being.[15–18] However, measurement of PFAS at the drinking water regulatory concentrations (in parts per trillion, ppt), [19] and at concentrations of certain environmental cleanup goals requires solid phase extraction to concentrate PFAS to the ppb (parts per billion) range so that they can be measured by liquid chromatography-tandem mass spectrometry (LC-MS/MS). These analytical techniques are complicated, expensive, and labor- and time-intensive.[20,21] The development of a low-cost and field-deployable detection method is therefore in high demand to test the presence of PFAS in remote or under-resourced locations.

Numerous existing techniques for PFAS analyses are reported in the literature. Among these, solid phase extraction (SPE)[22] combined with high-performance liquid chromatography (HPLC)[23] is highly regarded for its exceptional sensitivity and specificity, making it a reliable choice for detecting PFAS. While it requires specialized skills and experienced personnel, it remains a gold standard in laboratory settings. Portable electrochemical sensors offer a more accessible alternative, leveraging advanced nanomaterials[24] and conductive polymers[25] to enable real-time, on-site detection at lower costs.

In contrast to these methods, our objective is to present a simplified approach where a 2D thin film of eGaIn is leveraged to detect the presence of PFAS by assessing the physico-chemo-mechanical changes at the interface. We begin by shearing a droplet of eGaIn into a 2D thin film, quantifying its surface composition, and then determining the induced changes by dispensing PFAS droplets of varying concentrations. Introducing droplets of varying PFAS concentrations onto the 2D thin film, we noticed delamination, which we quantified using energy-dispersive X-ray (EDS) and Raman

[a] Department of Chemical and Materials Engineering, University of Nevada, Reno.
[b] Department of Chemistry, University of Nevada, Reno.
[c] Department of Mechanical Engineering, University of Nevada, Reno.
[d] Department of Civil & Environmental Engineering, University of Nevada, Reno.
*Corresponding Author: mrkhan@unr.edu
Supplementary Information available: [details of any supplementary information available should be included here]. See DOI: 10.1039/x0xx00000x

spectroscopies. We have further shown that the chemical activity and mechanical stability of a 2D eGaIn film are determined by the Ga to O ratio at the interface. These ratios are perturbed by the interfacial interactions with PFAS droplets, which induce delamination. For rapid *in situ* analyses, our method can complement existing methods of detecting the presence of PFAS. With further studies and improvements, our approaches can contribute to developing low-cost chemical sensors for PFAS using LM alloys.

Experimental

Materials: Eutectic gallium indium-eGaIn (75% Ga, 25% In) was purchased from 5N Plus Trumbull Inc. The PFAS-contaminated waters were collected from Truckee (Lockwood 2 location, 0.0146ppb) and Walker River (Below Topaz Res. location, 0.001ppb). The 200 ppm PFOA solution was prepared in the lab using the PFOA powder (provided by Dr. Hiibel), and Deionized (DI) water (18 megaohms) was used throughout the experiment.

Bioanalytical grade Silicon wafers of N/Phosoprus type polished surface (Diameter 76,2+/-0,5mm; Thickness 380+/-25 microns) were purchased from SPW Industrial. For test fluids, Ethanol-denatured, anhydrous 94.9-96.0% (CAS no. 64-17-5) were purchased from VWR. DI water (18 megaohms) was available through the DI water supply system in the lab. A scanning electron microscope (SEM) (model-JSM-7100FT FESEM) was used for high-resolution imaging, which is available at the electron microscopy and microanalysis facility at UNR. All the images were analyzed using ImageJ software (NIH), and the figures were prepared in CorelDraw. Biorender was used to produce some of the images.

Methods

Thin Film Sample Preparation: Initially, we started with a bare silicon wafer. In order to clean it properly, we plasma-treated the surface using Plasma-Etch. After that, using Ink Scape software, we drew two parallel straight-line patterns of ~2.5 cm at ~0.5 cm distance. We adjusted a fresh cotton swab with the XY plotter. Then, we adjusted the height of it. We placed the plasma-treated silicon wafer under the cotton swab and added two droplets of ~5µL of liquid metal at the points where the lines would start.

We brought a fresh cotton swab in close contact with the droplet and precisely positioned it so that the droplet was gently squashed into a flat shape. Then, the droplet was stretched 20 times to create a thin film on the silicon wafer. As the patterning on the silicon wafer was complete, we cut the patterned silicon wafer into small pieces and collected them in a petri dish, as shown in **Figure 1 (b-c)**.

Thin Film Characterization (SEM & AFM):

For thin film characterization, we initially utilized two methods. We looked into the topography of the fabricated thin film using Scanning Electron microscope (model-JSM-7100FT FESEM). For sample preparation, a small sample was cut and placed in an SEM sample holder using double-sided carbon tape. During imaging, we zoomed into multiple magnifications to look for different features in the thin film. It has been shown in **Figure 1 (d-e)**.

A commercial AFM instrument (MFP-3D Infinity by Asylum Research) was employed to assess both the surface topography and film thickness of a deposited liquid metal layer. All topographical images were acquired in tapping mode using a silicon cantilever with an aluminum reflective coating and a nominal stiffness of 0.2 nN/nm (BudgetSensor). Given the film's low stiffness, scans were conducted in net-attractive mode to minimize tip-sample interaction forces, with the scan rate carefully regulated at 0.5 Hz for both the figures [1(f) and 1(i)]. Multiple scans were performed to capture essential film features, including small deposition regions and the height difference between the film and substrate. The thin film thickness was quantified, showing a range of approximately 1.1 to 1.5 µm [Figures 1(f-g) and Figure S2]. In some areas, localized gallium (Ga) accumulation was detected, resulting in a thickness increase of around 500 nm compared to the surrounding flat film regions, as illustrated in Figures 1(h-i).

Raman Analyses: Raman spectroscopy analyses were performed at the University of Nevada, Reno, utilizing a Horiba LabRAM HR Evolution spectrometer configured for a spectral range of 10–4000 nm. The system included an open-space confocal microscope, a Märzhäuser *x-y* motorized stage, two diffraction gratings (600 and 1800 grooves/mm), and a multichannel Syncerity 1024 × 256 Open Electrode (OE) charge-coupled device (CCD) detector, which provided a broad range of spectral resolution. A 50x or 100× objective lens with a 0.9 numerical aperture was used for measurements, which were calibrated with a 520.6 cm–1 silicon standard. Excitation was provided by a frequency-doubled Nd: YAG laser (Oxxius, France) operating at 532 nm, resulting in a beam diameter of 1 µm. Neutral density filters were employed to typically adjust the laser power to 50% of the maximum output. Signal acquisition time was ~40 s for 2 accumulations within 10 to 4000 nm wavelength. Each measurement spot was inspected optically before collecting Raman spectra. To achieve an optimal signal-to-noise ratio (SNR), with background noise ideally less than 1% of the signal, measurements were conducted using a 200 µm confocal hole and by adjusting the neutral density (ND) filter. Fluorescence was mitigated by rotating the sample, reducing the confocal hole size, or adjusting the laser power using the ND filter.

To perform Raman analysis on the thin film, we initially took a small silicon wafer sample with an LM pattern on it. Then, we dispensed a ~3µL droplet on top of the thin film and dried it for 2 mins on a hot plate at 70°C. Then, we placed it under the microscope associated with Raman and ran the analysis to collect the absorbance peaks.

Image analysis using ImageJ: We used image analysis to calculate the number of pinholes as well as the area of delamination on the LM pattern. The first step for this sort of analysis is to define the scale from the existing image. Then, we converted the image into an 8-bit binary image and modulated the threshold so that there was a high contrast between the LM and LM free spaces. Then, from the Analyze menu, we can select analyze particles and adjust the setting as per requirement to have the measure on a specific area.

List of acronyms related to PFAS

PFAS	per and polyfluoroalkyl substances
PFBA	perfluorobutanoic acid

PFBS	perfluorobutanesulfonic acid
PFHxS	perfluorohexane sulfonate
PFHxA	perfluorohexanoic acid
PFHpA	perfluoroheptanoic acid
PFOA	perfluorooctanoic acid
PFOS	perfluorooctanesulfonic acid
ppb	parts per billion
ppm	parts per million
ppt	parts per trillion

Result and Analysis

Using a cotton swab mounted on an XY plotter, we shear thinned[26] a droplet of ~5 µL eGaIn onto a plasma-treated (oxygen) silicon wafer and produced a thin film. As we add the droplet to the silicon wafer surface, the bare metal does not wet the silicon wafer and initially adopts a perturbed shape to minimize surface energy. [27]

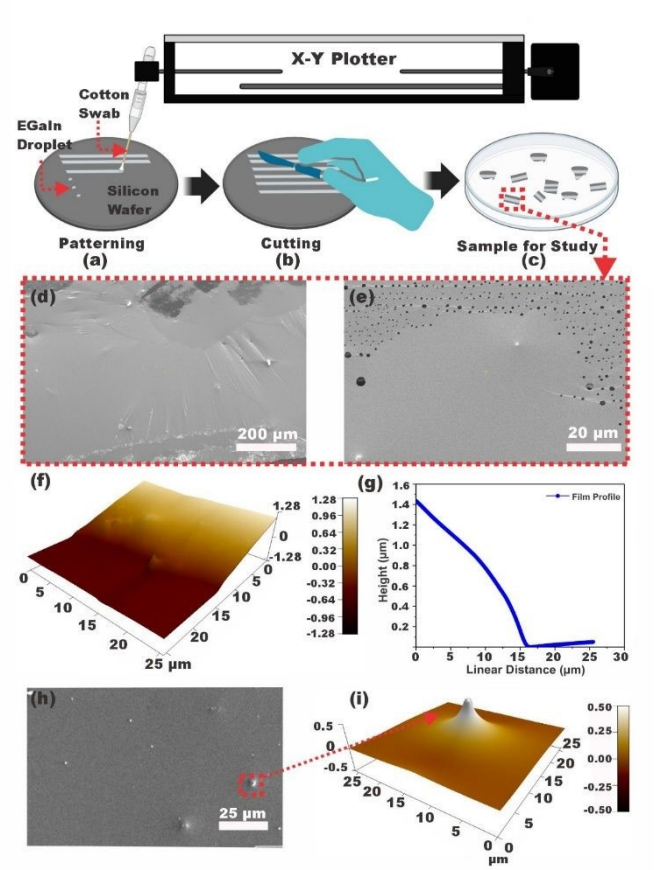

Figure 1: Depiction of 2D eGaIn film generation on a silicon wafer. Cartoon depiction of (a) creating eGaIn pattern using cotton swab utilizing an XY plotter, (b) cutting the thin film patterned silicon wafer into small pieces shown in (c), (d) topography of a small sample under scanning electron microscope (SEM) at 200X magnification, (e) topography of the small sample under scanning electron microscope (SEM) at 2000X magnification. Thickness measurement of eGaIn thin film using AFM. (f) AFM topography of eGaIn thin film sample denoting a thickness of ~ 1.4 µm, (g) graphical representation of eGaIn thin film sample denoting a thickness of ~ 1.4 µm, (h) SEM topography of the sample area where liquid gallium was accumulated creating bumps, (i) AFM topography of the sample area where liquid gallium was accumulated having a bump of ~0.5 µm thickness.

We brought a fresh cotton swab in close contact with the droplet and then precisely positioned it with an XY plotter to compress it gently and strain it into a thin film. The tip's position and motion during the drag were pre-programmed in the XY plotter. The width of the film was defined by the wetted area of the tip, which we did not try to control. Then, the droplet was stretched 20 times to create a thin film having 25mm in length on the silicon wafer. The entire process is shown in Figure 1a. Once the patterning on the silicon wafer was complete, we cut the patterned silicon wafer into small pieces and collected them in a Petri dish, as shown in Figure 1 (b-c).

Ga_2O_3 lowers the interfacial tension of the bare metal [11] and allows the bulk metal to be micromolded. [1,6] Ga_2O_3 also wets various surfaces with a few exceptions. [28] The cotton swab we used is a porous material (Fig S1), initially wetted by the oxides. As the cotton swab-mounted XY plotter thins the metal droplets, the oxide with a thin bare metal layer is mechanically pinned and stabilized with random heterogeneities throughout the film. The topography of the eGaIn film shown in Figure 1 (d-e) was measured using scanning electron microscopy (SEM) and was heterogeneous due to the random distribution of pinholes and other surface features.[27] However, as the oxide forms almost instantaneously in air, the produced thin film retains 2D shapes throughout the entire experimental observations. [10]

We quantified the thickness of the thin film produced using atomic force microscopy (AFM) due to its high resolution and sensitivity. The thickness was between ~1.1-1.5 µm [Figure 1(f-g) & Fig S2]. In some places, we noticed the accumulation of Ga, where the thickness was higher by ~500 nm compared to the flat, thin film area, as shown in Figure 1(h-i).

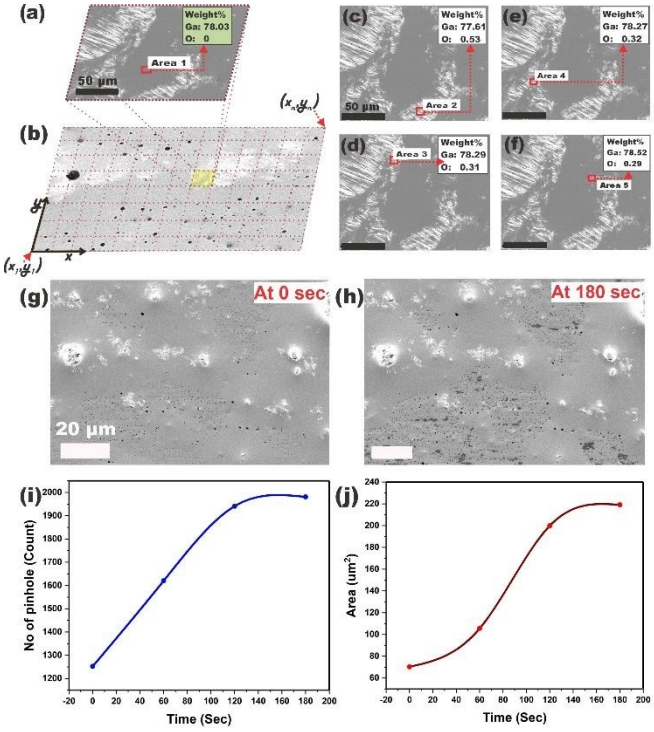

Figure 2: Elemental Analysis on eGaIn film. (a) topography and EDS data of eGaIn thin film sample identifying the targeted area where the amount of oxygen is zero, (b) broader topography of thin film indicating from where the region in (a) was obtained, (c), (d), (e), and (f) topography and EDS data of eGaIn thin film sample identifying targeted area surrounding area shown in (a) where the amount of oxygen is non zero, (g) acquired an image of a pinhole onto eGaIn thin film area, (h) additional image of

pinhole generation onto eGaIn thin film area after 180 seconds, (i) quantitative data on the number of pinholes generated over time, (j) quantitative data on the pinhole area increased over time. The scale bars in (a-f) are 50 µm, and the scale bars in (g-h) are 20 µm.

Numerous methods are currently reported to produce 2D thin films of eGaIn.[29,30] However, we preferred the technique we described here and used before due to the (i) control over easy fabrication of 2D thin film and (ii) generation of random heterogeneities across the entire film, which we would like to investigate for interfacial studies.[10] We used SEM at a low accelerating voltage (~2kV) of electrons to monitor the thin film's strain relaxation, quantify the number of pinholes, and determine the elemental composition of Ga and O across the thin film, as shown in Figure 2b. We observed a variable distribution of O and Ga across the sample area. Figure 2a shows the distribution of one such area. Elemental analysis using energy-dispersive X-ray spectroscopy (EDS) revealed a different spatial distribution, with regions lacking oxygen surrounded by oxygen-enriched areas. This observation suggests we can create a mixed metal oxide layer, which introduces a random distribution of Ga and O, forming a non-stoichiometric Ga_XO_Y (here, X and Y values depend on elemental composition in EDS analyses) layer. Figures 2(c-f) represent some areas where we noticed variations in Ga and O compositions and a continuous formation of pinholes, as shown in Figure 2(g-h) at the 2 kV electron acceleration voltages.

We captured a sequence of SEM images at 2 kV acceleration voltage and then used ImageJ to analyze the number of pinholes and areas covered by the pinholes, as shown in Figure 2(i-j). More Ga and O were found around the edges of the pinholes than in adjacent areas, which suggests that oxide is pinned near the edge of the pinholes. However, pinholes might be generated due to a mismatch in interfacial tension between the oxide and bare metal[11]. Also, we noticed new pinholes and pinhole enlargement over time. While interfacial tension mismatch is likely the true cause of pinhole dynamics, we primarily focus on interfacial interactions, leveraging the surface heterogeneities in this article. However, the literature has reported that molten metal droplets' impact on solid substrates may entrap gas to form pinholes[31]. This gas entrapment and contact line retraction may cause single or multiple pinholes. During fabrication, there is a chance of entrapped air between the cotton swab's porous, non-woven fibrous structure and the oxide layer of eGaIn. However, these entrapped gases are not visible using optical microscopy but are progressively revealed at low-acceleration voltages in SEM. In contrast, these entrapped gases will likely expand and burst under a vacuum. We did not notice such expansion and burst events; rather, we found an increase in pinholes over time, which induced more heterogeneities at the surface. Pinholes in thin metal films like iron, copper, and silver often occur during deposition techniques such as PVD (physical vapor deposition techniques such as sputtering or evaporation) due to uneven nucleation and coverage.[32,33] Surface imperfections and thermal stress can also lead to pinholes, impacting film quality.[34,35] Pinhole formation in eGaIn or gallium alloy thin films and oxide may result from the combined effects of surface tension, strains, and their chemical reactions.[36]

We hypothesize that the stability of the produced thin film is perturbed by the interfacial interactions occurring at the top surface with different analytes, inducing a differential shift in the Ga vs. Ga/O ratio. We leverage Raman spectroscopies to quantify such physico-chemo-mechanical shifts. For simplicity, we will denote the thin films of eGaIn as "active material" in the subsequent sections, as it enables sensing the presence of adsorbed analytes. We have utilized DI water and 100 PPT PFOA on pristine Si wafer as control fluids to begin our PFAS studies.

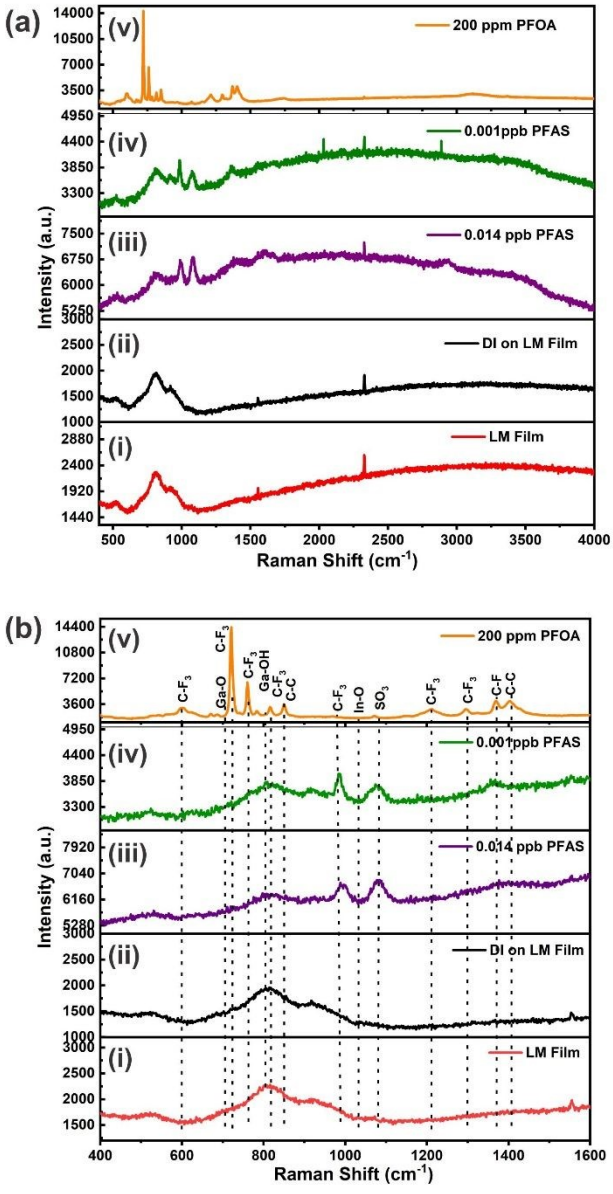

Figure 3: Raman spectrum of liquid metal (eGaIn) thin film while exposed to different concentrations of PFAS/PFOA. (a) Raman absorbance peaks observed for different fluid droplets on eGaIn thin film (global scan), (b) Raman absorbance peaks observed on (i) bare LM, (ii) after adding DI water (iii) after adding 0.014 ppb PFAS water (iv) after adding 0.001ppb PFAS water, (v) after adding 200 ppm PFOA water.

We used Raman spectroscopy to determine the adsorption of PFAS solutions (such as 0.001 ppb PFAS, 0.014 ppb PFAS, and 200 ppm PFOA) and reference fluid (DI water) onto the active material, as shown in Figure 3(a). For these experiments, the Raman spectra obtained in Figure S5i and S5iii are used as a control. We compared these results to the spectra obtained from a thin film of liquid metal (eGaIn) patterns on a Si wafer [Figures 3a(i) and 3b(i)]. For that, we treated the Si wafer with oxygen plasma and then produced the thin LM film (active material) on the Si wafer. Then, we introduced 3 µL droplets of different PFAS solutions and reference fluids on the LM pattern and dried them at 70°C using a hot plate before performing Raman spectroscopy.

Raman spectroscopy probes the vibrational modes of molecules or crystals, which are sensitive to chemical environment and structure.[37] It provides useful information on the surface chemistry of the active material used in this study. As mentioned before, in the presence of air, the surface of eGaIn is coated with a ~3 nm thick layer of Ga_2O_3. The surface heterogeneities of the eGaIn thin film in air and the dynamics of Ga_2O_3 would allow chemical analyses of microdroplets with foreign analytes. When PFAS solution or reference fluids are introduced to Ga_2O_3, the representative Raman shift of Ga_2O_3 changes. Therefore, to understand the interaction between Ga_2O_3 and PFAS, observing Raman interactional shifts would be instrumental. Our fabricated thin films were exposed to different PFAS solutions containing fluorinated analytes and reference fluids containing hydroxyl radicals in the current study. Considering the eGaIn pattern as the reference in Figure 3, we compared the shift after adding those analytes to the LM pattern. The Raman spectrum of the Si wafer exhibits peaks at 522, 980, 2327, and 3072 cm^{-1} [Figure S5(i)]. When the Si wafer surface is covered with eGaIn, peaks are observed at 522, 788, 989, and 2327 cm^{-1}. As we zoomed in more into the peaks in Figure 3b(i), we found two nearby peaks at ~706 and ~804 cm^{-1}, which indicate the presence of Ga_2O_3 and Ga-O-H.[38] To compare these results, Raman spectra of plasma-cleaned Si wafer, DI water on plasma-cleaned Si wafer, and 100 ppt PFOA on plasma-cleaned Si wafer as controls are given in Figure S5. The Raman spectrum of the bare Si wafer exhibits peaks of transverse acoustic (TA) mode at ~52 cm^{-1}, the longitudinal acoustic (LA) mode at ~297 cm^{-1}, the longitudinal optical (LO) mode at ~429 cm-1, and the transverse optical (TO) mode at ~513 cm^{-1}. Additionally, Si-H wagging/rocking vibration modes in different bond topologies produced a little peak at ~612 cm^{-1}. The Si-O bond vibrations are typically attributed to another peak at ~925 cm^{-1}. This result is consistent with a previous study.[39] There are no more peaks observed after adding DI water and 100 ppt PFOA on the Si wafer surface.

We conducted Raman analyses for 3 different samples of PFAS-contaminated water, one of which was spiked in the lab (200 ppm PFOA) and two of which were collected from contaminated environmental sources (0.001 ppb PFAS, primarily PFHxS and PFOS, and 0.014 ppb PFAS, primarily PFBS, PFHpA, PFHxS, PFHxA, PFOS and PFOA). Figure 3a,b(iii-v) show the associated Raman spectra. Despite substantial differences in the organic makeup of these samples[40] we identified a co-occurring peak at ~600, 723, 763 and 819 cm^{-1}, corresponding to the $\delta(CF_3)$ vibration.[41,42] These co-occurring spectral signatures provide valuable insights into the interaction between PFAS and the eGaIn film, but also provide evidence that the method is capable of detecting PFAS in complex matrices containing various salts and organic compounds. We observed two peaks around ~1210 and 1300 cm^{-1}, corresponding to the stretching vibration of the trifluoromethyl (CF_3) group $\nu(CF_3)$.[41] Furthermore, peaks corresponding to the stretching vibrations of the carbon-fluorine bond ν(CF) at ~1370 cm^{-1} and the carbon-carbon bond (ν(CC)) in the range of ~ 1406 cm^{-1} were also identified. Only in the case of the first two samples (0.001 ppb PFAS, then 0.014 ppb PFAS), we observed the peak for $\nu(SO_3)$ between 1050-1170 cm^{-1}.[41] This peak was missing in the case of the 200 ppm PFOA sample. We cross-validated these peaks with existing literature on PFOA and PFOS. [41] More details on the Raman spectra of Figures 3a,b(iii-v) are given in the supplemental section. These spectral signatures provide valuable insights into the molecular interactions between PFAS and the eGaIn thin film.

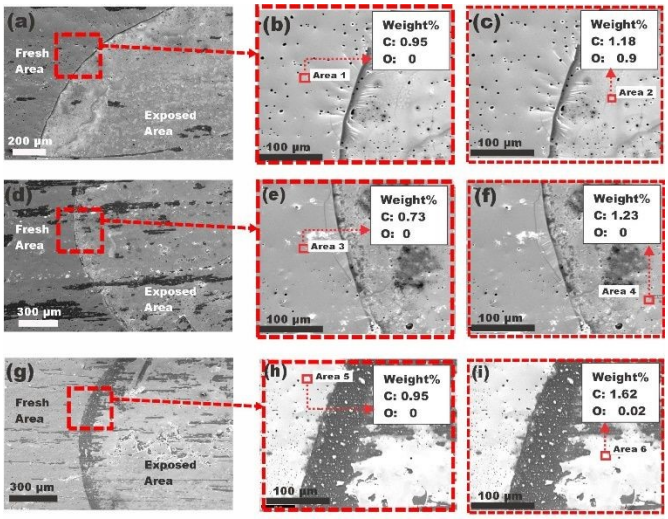

Figure 4: SEM Topography and EDS of liquid metal (eGaIn) thin film after exposure to varying PFAS concentrations. (a) topography of a eGain thin film exposed to 0.001 ppb PFAS under scanning electron microscope (SEM) at 150X magnification, (b) quantitative data of carbon and oxygen on the fresh side of the film using EDS, (c) quantitative data of carbon and oxygen on the that was side exposed to 0.001 ppb PFAS using EDS shows the increased quantity of carbon and oxygen, (d) topography of a eGain Thin film exposed to 0.014 ppb PFAS under scanning electron microscope (SEM) at 120X magnification, (e) quantitative data of carbon and oxygen on the fresh side of the film using EDS, (f) quantitative data of carbon and oxygen on the that was side exposed to 0.014 ppb PFAS using EDS shows the increased quantity of carbon and oxygen, (g) topography of a eGain Thin film exposed to 200 ppm PFOA under scanning electron microscope (SEM) at 80X magnification, (h) quantitative data of carbon and oxygen on the fresh side of the film using EDS, (i) quantitative data of carbon and oxygen on the that was side exposed to 200 ppm PFOA using EDS shows the increased quantity of carbon and oxygen.

The shifts in Raman spectra in Figure 3 suggest that the eGaIn thin films can be used for analyte detection. In addition to chemical sensitivities and peak shifts, we also noticed delamination of the thin films at varying concentrations of the analytes. This phenomenon can be attributed to the surface-active nature of PFAS molecules, which lowers the surface tension of the droplets and alters the interfacial

DOI: 10.1039/D5CP00485D

forces.[43] To understand this phenomenon, we analyzed these samples using SEM. As we added the droplets to the film of liquid metal, the extent of delamination at the droplet edge varied significantly with the concentration of PFAS/PFOA in the droplets. Initially, we added a droplet of deionized (DI) water as a control and found no delamination on the film's surface, suggesting that the liquid metal film remained largely intact and stable under this condition, as shown in Figure S6 (j-l). However, with the introduction of PFAS solutions, even at an extremely low concentration of 0.001 ppb, presented in Figures 4 (a-c) and S6 (a-c), the film started to delaminate at the edge of the droplet. This trend continued as the PFAS concentration was raised to 0.0146 ppb in Figure 4(d-f) and Figure S6 (g-i) and then dramatically at 200 ppm, shown in Figure 4(g-i), in which substantial delamination was observed. We calculated the degree of delamination by measuring the area impacted in ImageJ. In the case of a 200 ppm PFOA-contaminated water droplet, for a 246,500 μm^2 film area, the delaminated area was found to be 95,788 μm^2. This corresponds to a 38% delamination of the film. In the 0.001 ppb and 0.014 ppb PFAS samples, 3.33% and 10.53% film delamination were observed. The delamination of the liquid metal film increased with higher concentrations of PFAS droplets, while lower concentration droplets resulted in less delamination. Briefly, the chemical sensitivity using Raman spectra and mechanical stability using EDS-ImageJ analyses suggest that a heterogeneous thin film of eGaIn can sense and detect dilute concentrations of PFAS on demand.

Conclusions

In this study, we explored the chemical interaction of eGaIn thin film surfaces, demonstrating their capability to interact with different concentrations of PFAS. By examining how dilute amounts of PFAS affect the mechanical stability and shift the chemical composition of liquid metal films, we have expanded the basic and applied knowledge of liquid metal thin films in environmental technologies – especially water technologies.

Our study demonstrated that a 2D thin film of liquid metal exhibits a variable distribution of O and Ga across the sample surface. We found enhanced chemical activity in the film, where differential oxide- and gallium-enriched areas exhibit regions of pinholes, offering the potential for harnessing these regions for analyte detection. Such surface sites could provide unique opportunities to study molecular interactions *in situ*. We showed that the inherent chemical activity of the surface facilitates the interaction with molecules. Raman spectroscopy provided further insights, showing significant shifts in peaks, indicating PFAS molecules' adsorption onto the liquid metal film. The adsorption process likely introduces additional stress at the interface, contributing to the observed delamination. However, we did not focus on the interfacial stress measurements in this study.

We explored physico-chemo-mechanical changes upon introducing droplets of DI water and PFAS solutions with varying concentrations (0.001 ppb, and 0.0146 ppb) and 200 ppm PFOA onto the film. The DI water droplet did not cause delamination, indicating that the liquid metal film remained relatively stable under this condition. However, as the concentration of PFAS increased, the delamination area expanded significantly. This can be attributed to the surface-active nature of PFAS molecules. The increased delamination with higher PFAS concentrations suggests a method for tuning the film's response by controlling the PFAS concentration, indicating the chemical-sensitive nature of the thin film. We need additional investigations to find the exact reasons for the delamination. However, the insights gained should contribute to developing liquid metals-based chemical sensors for sensitive and selective analyte detection, offering a novel approach to chemical sensing that can improve the detection of contaminants and other analytes in various applications.[44]

Author contributions

M.R.K. conceptualized the idea, managed support, mentored, and coordinated, and M.M. and M.S.M experimented and validated it. Dr. Hanigan provided field samples of PFAS. Dr. Barile provided Raman, and Dr. Tung provided AFM. All authors contributed to executing the idea, assisted in experiments, revised the manuscript, and finalized the draft.

Conflicts of interest

This idea has been filed for a provisional patent application by the University of Nevada, Reno.

Data availability

Data requests should be directed to the corresponding author.

Acknowledgments

This research was funded under a Cooperative Agreement with the U.S. Army Corps of Engineers, Engineer Research and Development Center, and Construction Engineering Research Laboratory (USACE ERDC-CERL), under the contract W91T32T-23-2-0004 (Advanced Technologies for Water Reuse, 2023) through the Nevada Center for Water Resiliency (NCWR). P. M. and C. J. B. acknowledge support from the National Science Foundation CAREER Award under Grant No. CHE-2046105.

References

1 R. C. Chiechi, E. A. Weiss, M. D. Dickey and G. M. Whitesides, Eutectic Gallium–Indium (EGaIn): A Moldable Liquid Metal for Electrical Characterization of Self-Assembled Monolayers, *Angewandte Chemie International Edition*, 2008, **47**, 142–144.

2 F.-M. Allioux, M. B. Ghasemian, W. Xie, A. P. O'Mullane, T. Daeneke, M. D. Dickey and K. Kalantar-Zadeh, Applications of

liquid metals in nanotechnology, *Nanoscale Horiz.*, 2022, **7**, 141–167.
3 S.-Y. Tang, C. Tabor, K. Kalantar-Zadeh and M. D. Dickey, Gallium Liquid Metal: The Devil's Elixir, *Annual Review of Materials Research*, 2021, **51**, 381–408.
4 S. Amini, X. Chen, J. Q. I. Chua, J. S. Tee, C. A. Nijhuis and A. Miserez, Interplay between Interfacial Energy, Contact Mechanics, and Capillary Forces in EGaIn Droplets, *ACS Appl. Mater. Interfaces*, 2022, **14**, 28074–28084.
5 J.-H. Kim, S. Kim, M. D. Dickey, J.-H. So and H.-J. Koo, Interface of gallium-based liquid metals: oxide skin, wetting, and applications, *Nanoscale Horiz.*, DOI:10.1039/D4NH00067F.
6 M. D. Dickey, Emerging Applications of Liquid Metals Featuring Surface Oxides, *ACS Appl. Mater. Interfaces*, 2014, **6**, 18369–18379.
7 I. D. Joshipura, H. R. Ayers, C. Majidi and M. D. Dickey, Methods to pattern liquid metals, *Journal of materials chemistry c*, 2015, **3**, 3834–3841.
8 E. S. Elton, T. C. Reeve, L. E. Thornley, I. D. Joshipura, P. H. Paul, A. J. Pascall and J. R. Jeffries, Dramatic effect of oxide on measured liquid metal rheology, *Journal of Rheology*, 2020, **64**, 119–128.
9 T. Daeneke, K. Khoshmanesh, N. Mahmood, I. A. De Castro, D. Esrafilzadeh, S. J. Barrow, M. D. Dickey and K. Kalantar-Zadeh, Liquid metals: fundamentals and applications in chemistry, *Chemical Society Reviews*, 2018, **47**, 4073–4111.
10 K. Z. Hossain, M. Monwar and M. Rashed Khan, Reactive etching of gallium oxide on eutectic gallium indium (eGaIn) with chlorosilane vapor to induce differential wetting, *Soft Matter*, 2023, **19**, 3199–3206.
11 M. R. Khan, C. B. Eaker, E. F. Bowden and M. D. Dickey, Giant and switchable surface activity of liquid metal via surface oxidation, *Proc Natl Acad Sci USA*, 2014, **111**, 14047–14051.
12 M. R. Khan, C. Trlica and M. D. Dickey, Recapillarity: Electrochemically Controlled Capillary Withdrawal of a Liquid Metal Alloy from Microchannels, *Advanced Functional Materials*, 2015, **25**, 671–678.
13 C. B. Eaker and M. D. Dickey, in *Micro- and Nanotechnology Sensors, Systems, and Applications VII*, SPIE, 2015, vol. 9467, pp. 21–29.
14 M. D. Dickey, Stretchable and Soft Electronics using Liquid Metals, *Advanced Materials*, 2017, **29**, 1606425.
15 S. Y. Wee and A. Z. Aris, Environmental impacts, exposure pathways, and health effects of PFOA and PFOS, *Ecotoxicology and Environmental Safety*, 2023, **267**, 115663.
16 A. Voulgaropoulos, Mitigation of PFAS in U.S. Public Water Systems: Future steps for ensuring safer drinking water, *Environmental Progress & Sustainable Energy*, 2022, **41**, e13800.
17 J. Glüge, M. Scheringer, I. T. Cousins, J. C. DeWitt, G. Goldenman, D. Herzke, R. Lohmann, C. A. Ng, X. Trier and Z. Wang, An overview of the uses of per- and polyfluoroalkyl substances (PFAS), *Environ. Sci.: Processes Impacts*, 2020, **22**, 2345–2373.
18 M. G. Evich, M. J. B. Davis, J. P. McCord, B. Acrey, J. A. Awkerman, D. R. U. Knappe, A. B. Lindstrom, T. F. Speth, C. Tebes-Stevens, M. J. Strynar, Z. Wang, E. J. Weber, W. M. Henderson and J. W. Washington, Per- and polyfluoroalkyl substances in the environment, *Science*, 2022, **375**, eabg9065.
19 O. US EPA, Per- and Polyfluoroalkyl Substances (PFAS), https://www.epa.gov/sdwa/and-polyfluoroalkyl-substances-pfas, (accessed 7 October 2024).
20 L. J. Winchell, M. J. M. Wells, J. J. Ross, X. Fonoll, J. W. Norton, S. Kuplicki, M. Khan and K. Y. Bell, Analyses of per- and polyfluoroalkyl substances (PFAS) through the urban water cycle: Toward achieving an integrated analytical workflow across aqueous, solid, and gaseous matrices in water and wastewater treatment, *Science of The Total Environment*, 2021, **774**, 145257.
21 C. Wu, Q. Wang, H. Chen and M. Li, Rapid quantitative analysis and suspect screening of per-and polyfluorinated alkyl substances (PFASs) in aqueous film-forming foams (AFFFs) and municipal wastewater samples by Nano-ESI-HRMS, *Water Research*, 2022, **219**, 118542.
22 T. E. Lockwood, M. Talebi, A. Minett, S. Mills, P. A. Doble and D. P. Bishop, Micro solid-phase extraction for the analysis of per- and polyfluoroalkyl substances in environmental waters, *Journal of Chromatography A*, 2019, **1604**, 460495.
23 S. K. Selahle, A. Mpupa and P. N. Nomngongo, Liquid chromatographic determination of per- and polyfluoroalkyl substances in environmental river water samples, *Arabian Journal of Chemistry*, 2022, **15**, 103960.
24 R. Khan, Z. O. Uygun, D. Andreescu and S. Andreescu, Sensitive Detection of Perfluoroalkyl Substances Using MXene–AgNP-Based Electrochemical Sensors, *ACS Sens.*, 2024, **9**, 3403–3412.
25 M. H. Hassan, R. Khan and S. Andreescu, Advances in electrochemical detection methods for measuring contaminants of emerging concerns, *Electrochemical Science Advances*, 2022, **2**, e2100184.
26 E. S. Elton, T. C. Reeve, L. E. Thornley, I. D. Joshipura, P. H. Paul, A. J. Pascall and J. R. Jeffries, Dramatic effect of oxide on measured liquid metal rheology, *Journal of Rheology*, 2020, **64**, 119–128.
27 M. R. Khan, J. Bell and M. D. Dickey, Localized Instabilities of Liquid Metal Films via In-Plane Recapillarity, *Advanced Materials Interfaces*, 2016, **3**, 1600546.
28 S.-Y. Tang, C. Tabor, K. Kalantar-Zadeh and M. D. Dickey, Gallium Liquid Metal: The Devil's Elixir, *Annual Review of Materials Research*, 2021, **51**, null.
29 P. Aukarasereenont, A. Goff, C. Kim Nguyen, C. F. McConville, A. Elbourne, A. Zavabeti and T. Daeneke, Liquid metals: an ideal platform for the synthesis of two-dimensional materials, *Chemical Society Reviews*, 2022, **51**, 1253–1276.
30 A. Goff, P. Aukarasereenont, C. K. Nguyen, R. Grant, N. Syed, A. Zavabeti, A. Elbourne and T. Daeneke, An exploration into two-dimensional metal oxides, and other 2D materials, synthesised via liquid metal printing and transfer techniques, *Dalton Transactions*, 2021, **50**, 7513–7526.
31 H. Yi, L. Qi, J. Luo, Y. Jiang and W. Deng, Pinhole formation from liquid metal microdroplets impact on solid surfaces, *Appl. Phys. Lett.*, 2016, **108**, 041601.
32 J. Shen, J. Giergiel, A. K. Schmid and J. Kirschner, Surface alloying and pinhole formation in ultra-thin FeCu(100) films, *Surface Science*, 1995, **328**, 32–46.
33 A. Hadni and R. Thomas, The use of a regular distribution of minute pinholes for the epitaxial growth of an oriented thin film, *Thin Solid Films*, 1981, **81**, 247–256.
34 D. J. Fisher, *Liquid Metal Alloys in Electronics*, Materials Research Forum LLC, 2020.
35 P. C. Ohara and W. M. Gelbart, Interplay between Hole Instability and Nanoparticle Array Formation in Ultrathin Liquid Films, *Langmuir*, 1998, **14**, 3418–3424.
36 J. Yang, W. Cheng and K. Kalantar-zadeh, Electronic Skins Based on Liquid Metals, *Proc. IEEE*, 2019, **107**, 2168–2184.

View Article Online
DOI: 10.1039/D5CP00185D

37 A. B. S. Elliott, R. Horvath and K. C. Gordon, Vibrational spectroscopy as a probe of molecule-based devices, *Chemical Society Reviews*, 2012, **41**, 1929–1946.
38 W. Xie, F.-M. Allioux, R. Namivandi-Zangeneh, M. B. Ghasemian, J. Han, Md. A. Rahim, J. Tang, J. Yang, M. Mousavi, M. Mayyas, Z. Cao, F. Centurion, M. J. Christoe, C. Zhang, Y. Wang, S. Merhebi, M. Baharfar, G. Ng, D. Esrafilzadeh, C. Boyer and K. Kalantar-Zadeh, Polydopamine Shell as a Ga3+ Reservoir for Triggering Gallium–Indium Phase Separation in Eutectic Gallium–Indium Nanoalloys, *ACS Nano*, 2021, **15**, 16839–16850.
39 Y. Huang, Y. Zeng, Z. Zhang, X. Guo, M. Liao, C. Shou, S. Huang, B. Yan and J. Ye, UV-Raman scattering of thin film Si with ultrathin silicon oxide tunnel contact for high efficiency crystal silicon solar cells, *Solar Energy Materials and Solar Cells*, 2019, **192**, 154–160.
40 M. DeNicola, Z. Lin, O. Quiñones, B. Vanderford, M. Song, P. Westerhoff, E. Dickenson and D. Hanigan, Per- and polyfluoroalkyl substances and organofluorine in lakes and waterways of the northwestern Great Basin and Sierra Nevada, *Science of The Total Environment*, 2023, **905**, 166971.
41 B. M.b., N. Rhakho, S. R. Jena, S. Yadav, A. Altaee, M. Saxena and A. K. Samal, Detection of PFAS via surface-enhanced Raman scattering: Challenges and future perspectives, *Sustainable Chemistry for the Environment*, 2023, **3**, 100031.
42 J. C. Rothstein, J. Cui, Y. Yang, X. Chen and Y. Zhao, Ultra-sensitive detection of PFASs using surface enhanced Raman scattering and machine learning: a promising approach for environmental analysis, *Sens. Diagn.*, 2024, **3**, 1272–1284.
43 S. C. E. Leung, D. Wanninayake, D. Chen, N.-T. Nguyen and Q. Li, Physicochemical properties and interactions of perfluoroalkyl substances (PFAS) - Challenges and opportunities in sensing and remediation, *Science of The Total Environment*, 2023, **905**, 166764.
44 M. Monwar, K. Z. Hossain, G. Licup, T. Denton, J. Yoon and M. R. Khan, Liquid Metal in Expired Artificial Kidneys: A Nanoporous Soft Conductive Wire Platform for Unconventional Interfacial Fluidic Studies, *Adv Funct Materials*, 2024, **34**, 2307919.

View Article Online
DOI: 10.1039/D5CP00185D

Data availability

Data requests should be directed to the corresponding author